

FINITE ELEMENT METHOD FOR EPITAXIAL GROWTH WITH THERMODYNAMIC BOUNDARY CONDITIONS*

EBERHARD BÄNSCH[†], FRANK HAUSSER[‡], AND AXEL VOIGT[‡]

Abstract. We develop an adaptive finite element method for island dynamics in epitaxial growth. We study a step-flow model, which consists of an adatom (adsorbed atom) diffusion equation on terraces of different height; thermodynamic boundary conditions on terrace boundaries including anisotropic line tension; and the normal velocity law for the motion of such boundaries determined by a two-sided flux, together with the one-dimensional anisotropic “surface” diffusion (edge diffusion) of edge adatoms along the step edges. The problem is solved using independent meshes: a two-dimensional mesh for the adatom diffusion and one-dimensional meshes for the boundary evolution. A penalty method is used to incorporate the boundary conditions. The evolution of the terrace boundaries includes both the weighted/anisotropic mean curvature flow and the weighted/anisotropic edge diffusion. Its governing equation is solved by a semi-implicit front-tracking method using parametric finite elements.

Key words. epitaxial growth, island dynamics, free or moving boundary problem, adatom diffusion, surface diffusion, mean curvature flow, Gibbs–Thomson, finite elements, adaptivity, front tracking

AMS subject classifications. 35Q99, 35R35, 65N30, 65Z05, 74S05

DOI. 10.1137/030601028

1. Introduction. Epitaxial growth is a modern technology of growing single crystal films that inherit atomic structures from substrates. There are various kinds of models for epitaxial growth, among them the step-flow models of Burton–Cabrera–Frank (BCF) type; cf. [3, 4, 6, 11, 15, 20]. Here the description of the growth is continuous in the lateral directions but discrete in the growth direction. The model is essentially a free boundary problem that consists of a diffusion equation for the adatom density on islands, boundary conditions for the moving island boundaries, and an evolution equation for the island boundaries. If the attachment/detachment processes at the island boundaries are fast compared to the adatom diffusion on the islands (*diffusion limited growth*), the island boundaries act as perfect sinks for the adatoms. This is modeled by thermodynamic boundary conditions at the step edges. The evolution equation for the island boundaries considers not only mass balance but also edge diffusion, i.e., diffusion of edge adatoms along terrace boundaries.

Recently, level-set-based finite difference methods have been developed to solve the BCF equations in the diffusion limited regime [12, 5, 7, 19, 21]. In particular, in a layer-by-layer growth mode quantitative agreement with kinetic Monte Carlo simulations could be demonstrated. An alternative method based on a phase-field approach has been introduced in [18, 14, 22]. With both the level-set and the phase-field method, topological changes such as coalescence of islands can be handled very efficiently. But, until now, the (anisotropic) step energies and (anisotropic) edge diffusion have not been built in accurately. In particular it is not straightforward how

*Received by the editors September 29, 2003; accepted for publication (in revised form) November 8, 2004; published electronically July 13, 2005.

<http://www.siam.org/journals/sisc/26-6/60102.html>

[†]Numerical Mathematics and Scientific Computing, WIAS, Mohrenstraße 39, 10117 Berlin, Germany (baensch@wias-berlin.de).

[‡]Crystal Growth Group, Research Center caesar, Ludwig-Erhard-Allee 2, 53175 Bonn, Germany (hausser@caesar.de, voigt@caesar.de).

to discretize the fourth-order derivative occurring in the edge-diffusion term. Very recently, level-set approaches based on semi-implicit methods to describe such fourth-order evolution laws have been developed in [26, 9] but have not yet been applied to solve the BCF equations. A phase-field model which includes isotropic edge diffusion has been introduced only recently in [23].

Therefore, we see a need to introduce a method which is capable of treating anisotropic edge energies (i.e., weighted curvature in the boundary conditions) and anisotropic edge diffusion accurately. A framework for front-tracking finite element simulations of epitaxial growth with kinetic boundary conditions has been developed by the authors in [1]. Here we will extend the methods to also treat thermodynamic boundary conditions. Furthermore, the method is extended to include anisotropy. Even if coalescence of islands during growth cannot be handled with this approach at the moment, the method offers the possibility of studying the influence of step stiffness and edge diffusion during growth and coarsening of isolated islands or “nanomounds.” Here only trivial topological changes such as disappearance of islands occur, which can easily be handled by our front-tracking method.

As in [1], in developing our finite element method, we naturally divide our underlying problem into two parts: the adatom diffusion and the boundary evolution:

1. We derive a weak formulation for the time-dependent diffusion equation. To avoid the complexity of evaluating the adatom fluxes at the boundaries, boundary conditions are incorporated via a penalty method. The resulting equation is discretized using the linear finite element method. The arising linear system is symmetric positive definite, and thus is solved by the conjugate gradient method.
2. The geometric motion of the island boundaries includes both the mean curvature flow and the one-dimensional (1d) surface diffusion. It is treated in a variational formulation utilizing the curvature vector and discretized by a semi-implicit front-tracking method using parametric finite elements. This method is adapted with modification from [1, 2, 10] and extended to also handle anisotropy for both the mean curvature flow and the surface diffusion.

To obtain satisfactory computational results, meshes with sufficiently fine resolutions are needed for both the adatom diffusion equation and the boundary evolution equation. Thus, it is indispensable to use adaptivity for the method to be efficient. We use simple error indicators within an h -adaptive method to locally increase the spatial resolution.

We apply our method to the following test problems: (a) a purely geometric problem of the evolution of the boundaries that is governed by either the motion by weighted/anisotropic mean curvature or the motion by weighted/anisotropic 1d surface diffusion (edge diffusion). Our numerical results show the expected convergence to the Wulff shape, which is analyzed in detail; (b) the stability of a growing circular island. This problem has been analyzed rigorously in [16]. Our method yields numerical results that are in agreement with the theory. Besides these test problems, the method is used to study the influence of edge diffusion on anisotropic growth of a single island and the growth of a “wedding cake.” Furthermore, we present simulations concerning decay and coarsening. As a benchmark for long-time simulation, the fully two-dimensional (2d) simulation of the (isotropic) layer-by-layer decay of a (rotational symmetric) crystalline cone is compared with the numerical solution of the corresponding system of ODEs for the radii of the islands. Then Ostwald ripening of monolayer islands is investigated, and the theoretical scaling law for the average radius of the islands is reproduced by large-scale simulations. In the last two examples

simple topological changes occur due to the disappearance of islands, which can be handled easily by our numerical method.

In section 2, we describe the problem. In section 3, our methods of discretizing both the adatom diffusion equation and the boundary evolution equation and some implementational details are given. In section 4, we present our numerical results.

2. Problem description. Consider the dynamics of adatom islands in an epitaxially growing thin film. An island is a portion of crystal layer that is one atomic layer higher than the adjacent neighboring part of the film surface. Mathematically, we denote by $\Omega \subset \mathbb{R}^2$ the projected domain of the film surface in a 2d Cartesian coordinate system and assume that Ω is independent of time t . We denote also by $\Omega_0 = \Omega_0(t) \subset \mathbb{R}^2$ the projected domain of the substrate or the exposed film surface with the smallest layer thickness and denote by $\Omega_i = \Omega_i(t) \subset \mathbb{R}^2$, $i = 1, \dots, N$, the projected domain of the islands or terraces of relative height i at time t , respectively. Thus, $N + 1$ is the total number of layers that are exposed on the film surface. Note that, since the height of neighboring terraces differs only by one atomic layer, we conclude that $\overline{\Omega_i(t)} \cap \overline{\Omega_j(t)} = \emptyset$ if and only if $|i - j| \geq 2$. We denote further the corresponding island boundaries by $\Gamma_i(t) = \overline{\Omega_i(t)} \cap \overline{\Omega_{i-1}(t)}$, $i = 1, \dots, N$.

Denote by $\rho = \rho(x, t)$ the adatom density on Ω . The adatom diffusion on the terraces is described by the diffusion equation for the adatom density

$$(2.1) \quad \partial_t \rho - D \Delta \rho = F - \tau^{-1} \rho \quad \text{in } \Omega \setminus \bigcup_{i=1}^N \Gamma_i(t),$$

where $D > 0$ is the diffusion constant, $F > 0$ is the constant deposition flux rate, and $\tau^{-1} > 0$ is the constant desorption rate. Throughout this paper the unit of length will be the substrate lattice spacing. Thus the deposition rate F denotes the number of atoms deposited per unit time and adsorption site, and D is the ‘‘hopping rate.’’

We assume that the adatom density satisfies the following Gibbs–Thomson law on the island boundaries $\Gamma_i(t)$ for $i = 1, \dots, N$; see [15]:

$$(2.2) \quad \rho = \rho^* \left(1 + \frac{\tilde{\gamma} \kappa_i}{k_B T} \right),$$

where κ_i is the curvature of the boundary $\Gamma_i(t)$, ρ^* is a positive constant denoting the thermodynamic equilibrium density at straight steps, k_B is the Boltzmann constant, T is the temperature, and $\tilde{\gamma} = \gamma + \gamma_{\theta\theta}$ is the step stiffness of the boundary $\Gamma_i(t)$ related to the orientation-dependent step-free energy $\gamma(\theta)$ with θ , $0 \leq \theta \leq 2\pi$, the angle between the outer normal and the x_1 -axis.

For the motion of the steps, we assume the following law for the normal velocity v_i of the island boundary $\Gamma_i(t)$ for $i = 1, \dots, N$ (with the convention that $v_i > 0$ if the movement of Γ_i is in the direction of the unit normal \vec{n}_i pointing from upper to lower terrace):

$$(2.3) \quad v_i = -D[\nabla \rho \cdot \vec{n}_i]_i + \partial_s(\nu \partial_s(\tilde{\gamma} \kappa_i)),$$

where ν is a positive function denoting the (orientation-dependent) mobility for migration along edges [15, 6] and ∂_s denotes the tangential derivative along the boundary. For any function $u : \Omega \rightarrow \mathbb{R}$, $[u]_i = u^+ - u^-$ denotes the jump of u along $\Gamma_i(t)$ from the upper (+) to the lower (−) terrace. The term $\partial_s \nu (\partial_s(\tilde{\gamma} \kappa_i))$ represents the 1d (in general anisotropic/weighted) ‘‘surface’’ diffusion along the edges.

We assume a flux-free boundary condition for the adatom density on the boundary of the film domain:

$$(2.4) \quad \frac{\partial \rho}{\partial n} = 0 \quad \text{at } \partial\Omega \quad \forall t > 0,$$

where the normal derivative corresponds to the unit exterior normal \vec{n} to the boundary $\partial\Omega$. We also assume that the initial islands $\Omega_i(0)$ ($i = 0, \dots, N$) along with their corresponding boundaries $\Gamma_i(0)$ ($i = 1, \dots, N$) are given. Moreover, we assume that the initial adatom density is given by some function $\bar{\rho}$ on Ω . We assume compatibility of this initial value with the boundary condition (2.2), i.e.,

$$(2.5) \quad \bar{\rho}|_{\Gamma_i(0)} = \rho^* \left(1 + \frac{\tilde{\gamma}\kappa_i}{k_B T} \right),$$

for $i = 1, \dots, N$. Finally, we assume no topological changes in the dynamics; i.e., islands neither nucleate nor coalesce.

3. Variational formulation and finite element discretization. We derive a weak formulation for the time-dependent diffusion equation and use a first-order implicit scheme to discretize the time derivative. In each discrete time instant we perform the following steps: (1) we update the discrete boundaries by solving a geometric PDE based on the adatom densities and the discrete boundaries from the previous time step; (2) we solve the diffusion equation to update the adatom density using the adatom density from the previous time step and the computed discrete boundaries. In section 3.1, we describe the weak formulation for the time-dependent diffusion equation and the finite element discretization in each time step. In section 3.2, we present our algorithm for the geometric PDE of the boundary evolution.

3.1. Adatom diffusion. Assuming the boundaries $\Gamma_i(t)$ to be given, (2.1) may be viewed as a standard parabolic PDE with Dirichlet boundary conditions given on the “inner” boundaries $\Gamma_i(t)$ by (2.2). Nevertheless, there are two difficulties that have to be solved:

- (i) Since in the discretization the boundaries $\Gamma_i(t)$ are not part of the 2d mesh, it is not straightforward how to enforce the Dirichlet boundary conditions (2.2) directly.
- (ii) Solving the geometric PDE (2.3) involves the jump of the normal derivative of ρ at the boundaries $\Gamma_i(t)$.

To circumvent both difficulties, a penalty method is used. To this end assume that ρ is smooth inside each Ω_i . Multiplying both sides of the diffusion equation in (2.1) by a smooth, time-independent test function ϕ and integrating by parts, we get

$$(3.1) \quad \int_{\Omega} \partial_t \rho \phi + \int_{\Omega} D \nabla \rho \cdot \nabla \phi + \sum_{i=1}^N \int_{\Gamma_i(t)} D [\nabla \rho \cdot \vec{n}_i]_i \phi = \int_{\Omega} F \phi - \int_{\Omega} \tau^{-1} \rho \phi.$$

We now relax boundary condition (2.2) by a penalty method. More precisely, let $0 < \epsilon = \epsilon(x, t) \ll 1$ be given and replace (3.1) by

$$(3.2) \quad \int_{\Omega} \partial_t \rho \phi + \int_{\Omega} D \nabla \rho \cdot \nabla \phi + \sum_{i=1}^N \int_{\Gamma_i(t)} \frac{1}{\epsilon} \left(\rho - \rho^* \left(1 + \frac{\tilde{\gamma}\kappa_i}{k_B T} \right) \right) \phi = \int_{\Omega} F \phi - \int_{\Omega} \tau^{-1} \rho \phi.$$

Comparing (3.1) and (3.2), one concludes that a solution of (3.2) fulfills the following relaxed boundary condition on $\Gamma_i(t)$:

$$(3.3) \quad D[\nabla \rho \cdot \vec{n}_i]_i = \frac{1}{\epsilon} \left(\rho - \rho^* \left(1 + \frac{\tilde{\gamma} \kappa_i}{k_B T} \right) \right).$$

We will use this identity, when solving the geometric PDE (2.3) in section 3.2, to avoid the evaluation of $\nabla \rho \cdot \vec{n}_i$ at the boundaries $\Gamma_i(t)$.

We would like to mention that in the case of $\nu = 0$, i.e., without surface diffusion, the weak form (3.2) alternatively may be derived by adding a small velocity term in (2.2), giving

$$(3.4) \quad \rho = \rho^* \left(1 + \frac{\tilde{\gamma} \kappa_i}{k_B T} + \tilde{\epsilon} v_i \right).$$

Indeed, plugging (2.3) with $\nu = 0$ into (3.4) yields (3.3) with $\epsilon = \tilde{\epsilon} \rho^*$; cf. [24].

Now, split the time interval by discrete time instants $0 = t_0 < t_1 < \dots$ and define the time steps $\Delta t_m := t_{m+1} - t_m$ ($m = 0, 1, \dots$). Using the approximations $\Gamma_i^m \approx \Gamma_i(t_m)$, we have the following formulation of the time discrete problem.

PROBLEM 3.1. *Set $\rho^0 = \bar{\rho}$. For $m = 0, 1, \dots$, find adatom density $\rho^{m+1} \in H^1(\Omega)$ such that*

$$\begin{aligned} \int_{\Omega} \frac{\rho^{m+1} - \rho^m}{\Delta t_m} \phi + \int_{\Omega} D \nabla \rho^{m+1} \cdot \nabla \phi + \sum_{i=1}^N \int_{\Gamma_i^{m+1}} \frac{1}{\epsilon} \left(\rho^{m+1} - \rho^* \left(1 + \frac{\tilde{\gamma} \kappa_i^{m+1}}{k_B T} \right) \right) \phi \\ = \int_{\Omega} F \phi - \int_{\Omega} \tau^{-1} \rho^{m+1} \phi \quad \forall \phi_h \in H^1. \end{aligned}$$

To discretize in space, let \mathcal{T}_h^m be a conforming triangulation of Ω at time instant t_m . Define the finite element space of globally continuous, piecewise linear elements

$$\mathbb{V}_h^m = \{ v_h \in C^0(\bar{\Omega}) : v_h|_T \in \mathbb{P}^1 \quad \forall T \in \mathcal{T}_h^m \}.$$

Denote by $P_m : C^0(\bar{\Omega}) \rightarrow \mathbb{V}_h^m$ the usual Lagrange interpolation operator. With this setting, the space discretization of Problem 3.1 can be summarized as follows.

PROBLEM 3.2. *Let $\rho_h^0 = P_0 \bar{\rho}$. For $m = 0, 1, \dots$, determine the discrete adatom density $\rho_h^{m+1} \in \mathbb{V}_h^{m+1}$ by*

$$\begin{aligned} \int_{\Omega} \frac{\rho_h^{m+1} - \rho_h^m}{\Delta t_m} \phi_h + \int_{\Omega} D \nabla \rho_h^{m+1} \cdot \nabla \phi_h + \frac{1}{\epsilon(h)} \sum_{i=1}^N \int_{\Gamma_{i,h}^{m+1}} \left(\rho_h^{m+1} - \rho^* \left(1 + \frac{\tilde{\gamma} \kappa_i^{m+1}}{k_B T} \right) \right) \phi_h \\ = \int_{\Omega} F \phi_h - \int_{\Omega} \tau^{-1} \rho_h^{m+1} \phi_h \quad \forall \phi_h \in \mathbb{V}_h^{m+1}. \end{aligned}$$

Here κ_i^{m+1} are the discrete curvatures of $\Gamma_{i,h}^{m+1}$, and $\epsilon(h)$ with $\lim_{h \rightarrow 0} \epsilon(h) = 0$ is chosen to be constant on each element and to fulfill $\epsilon(h) = h/D$, which is an optimal choice for linear elements in elliptic problems [8, Ch. 3, sect. 3.2].

In the rest of this subsection, we fix a time step m and drop the subscript and superscript $m + 1$ when no confusion arises. Let $(\phi_k)_{k=1}^L$ be the standard nodal basis of the finite element space \mathbb{V}_h , where L is the dimension of \mathbb{V}_h . Expand ρ_h as

$$\rho_h^{m+1} = \sum_{k=1}^L r_k \phi_k$$

for some $R_i = (r_1, \dots, r_L)^t \in \mathbb{R}^L$. Define the following stiffness and mass matrices and load vectors:

$$\begin{aligned} \mathbf{M} &= (M_{kl}), & M_{kl} &= (\phi_k, \phi_l); & \mathbf{M}^{\Gamma_i} &= (M_{kl}^{\Gamma_i}), & M_{kl}^{\Gamma_i} &= \langle \phi_k, \phi_l \rangle_{\Gamma_i}; \\ \mathbf{A} &= (A_{kl}), & A_{kl} &= (D\nabla\phi_k, \nabla\phi_l); & \mathbf{F} &= (F_l), & F_l &= (F, \phi_l); \\ \mathbf{F}^{\Gamma_i} &= (F_l^{\Gamma_i}), & F_l^{\Gamma_i} &= \langle \rho^* (1 + \frac{\tilde{\gamma}\kappa_i}{k_B T}), \phi_l \rangle_{\Gamma_i}; \end{aligned}$$

where the index ranges are $1 \leq k, l \leq L$ and $\langle \cdot, \cdot \rangle_{\Gamma}$ stands for the L^2 inner product over the current interface Γ , whereas (\cdot, \cdot) denotes the L^2 inner product over the domain Ω . The following algorithm is the matrix form of Problem 3.2.

ALGORITHM 3.1. For $m = 0, 1, \dots$, find $R^{m+1} \in \mathbb{R}^L$ such that

$$\begin{aligned} \frac{1}{\Delta t_m} \mathbf{M} R^{m+1} + \mathbf{A} R^{m+1} + \frac{1}{\epsilon(h)} \sum_{i=1}^N \mathbf{M}^{\Gamma_i} R^{m+1} + \tau^{-1} \mathbf{M} R^{m+1} \\ = \mathbf{F} + \frac{1}{\epsilon(h)} \sum_{i=1}^N \mathbf{F}^{\Gamma_i} + \frac{1}{\Delta t_m} \mathbf{M} R^m. \end{aligned}$$

We introduce the following quantities defined on the nodes on the boundaries $\Gamma_{i,h}^{m+1}$:

$$(3.5) \quad \gamma_i := \frac{1}{\epsilon(h)} (\rho - \rho^*) = \frac{1}{\epsilon(h)} (\rho_h^{m+1}|_{\Gamma_{i,h}^{m+1}} - \rho^*).$$

These quantities will enter in the subproblem of the moving boundaries.

As already mentioned in section 2, the initial adatom density $\bar{\rho}$ (and therefore also the discrete initial adatom density ρ_h^0 in Problem 3.2) has to be compatible with the boundary conditions on the free boundaries Γ_i ; see (2.5). Moreover, the accuracy of the values of the adatom density is very important for the evolution of the free boundaries; see (3.5). Therefore we solve a separate problem to calculate suitable initial values ρ_h^0 . As in [24] we substitute the discrete time derivative in Problem 3.2 by $\rho_{t,h}^0 = 0$. We eventually arrive at the following problem to determine ρ_h^0 .

PROBLEM 3.3. For given initial polygonal curves $\Gamma_{i,h}^0$, $i = 1, \dots, N$, determine the initial discrete adatom density $\rho_h^0 \in \mathbb{V}_h^0$ as the solution of

$$\int_{\Omega} D\nabla\rho_h^0 \cdot \nabla\phi_h + \frac{1}{\epsilon(h)} \sum_{i=1}^N \int_{\Gamma_i^0} \left(\rho_h^0 - \rho^* \left(1 + \frac{\tilde{\gamma}\kappa_i^0}{k_B T} \right) \right) \phi_h = \int_{\Omega} F\phi_h - \int_{\Omega} \tau^{-1} \rho_h^0 \phi$$

for all $\phi_h \in \mathbb{V}_h^0$, with notation as in Problem 3.2.

Using the nodal basis and the mass and stiffness matrices as above, Problem 3.3 yields the following algorithm for the initial value.

ALGORITHM 3.2. Find $R^0 \in \mathbb{R}^L$ such that

$$\mathbf{A} R^0 + \frac{1}{\epsilon(h)} \sum_{i=1}^N \mathbf{M}^{\Gamma_i} R^0 + \tau^{-1} \mathbf{M} R^0 = \mathbf{F} + \frac{1}{\epsilon(h)} \sum_{i=1}^N \mathbf{F}^{\Gamma_i}.$$

3.2. Boundary evolution. Now assuming the adatom density ρ to be given, we use the identity (3.3) to avoid the direct evaluation of $\nabla\rho \cdot \vec{n}_i$ at the boundaries

$\Gamma_i(t)$ in the velocity law in (2.3). Thus we get the following geometric PDE for the boundary evolution of the moving boundaries Γ_i , $i = 1, \dots, N$:

$$(3.6) \quad v_i = \frac{1}{\epsilon}(\rho - \rho^*) - \frac{1}{\epsilon}\rho^* \frac{\tilde{\gamma}\kappa_i}{k_B T} + \partial_s(\nu\partial_s(\tilde{\gamma}\kappa_i)).$$

This equation can be interpreted as an equation for (weighted/anisotropic) surface diffusion with lower-order terms if $\nu > 0$ or for the (weighted/anisotropic) mean curvature flow with a forcing term if $\nu = 0$. A variational formulation and discretization by parametric finite elements for such a highly nonlinear fourth-order ($\nu > 0$) or second-order ($\nu = 0$) equation was given in [1] (for the isotropic case, i.e., $\nu = \text{const}$ and $\gamma = \text{const}$). We will now recall this formulation and modify it to also handle anisotropy.

By introducing the position vector \vec{x}_i , the curvature vector $\vec{\kappa}_i$, and the velocity vector \vec{v}_i , a system of equations for $\vec{\kappa}_i$, κ_i , v_i , and \vec{v}_i can be derived. By the geometric identity $\vec{\kappa}_i = -\partial_{ss}\vec{x}_i$, the velocity law (3.6), and the relations between the vector valued and scalar quantities $\kappa_i = \vec{\kappa}_i \cdot \vec{n}_i$ and $\vec{v}_i = v_i\vec{n}_i$, we obtain

$$(3.7) \quad \vec{\kappa}_i = -\partial_{ss}\vec{x}_i,$$

$$(3.8) \quad \kappa_i = \vec{\kappa}_i \cdot \vec{n}_i,$$

$$(3.9) \quad v_i = f_i,$$

$$(3.10) \quad \vec{v}_i = v_i\vec{n}_i,$$

where

$$f_i := \frac{1}{\epsilon}(\rho - \rho^*) - \frac{1}{\epsilon}\rho^* \frac{\tilde{\gamma}\kappa_i}{k_B T} + \partial_s(\nu\partial_s(\tilde{\gamma}\kappa_i)).$$

Consider the discrete time instant t_m and time step $\Delta t_m := t_{m+1} - t_m$ as in section 3.1. We represent the next free boundary Γ_i^{m+1} in terms of the current boundary Γ_i^m by updating the position vectors

$$(3.11) \quad \vec{x}_i \leftarrow \vec{x}_i + \Delta t_m \vec{v}_i.$$

The time discretization assumes that all geometric quantities such as \vec{n}_i , ∂_s are evaluated on the *current* free boundaries Γ_i^m . In contrast to the geometric quantities, the unknowns $\vec{\kappa}_i$, κ_i , v_i , and \vec{v}_i are treated implicitly. In particular, in view of (3.11), we define

$$(3.12) \quad \vec{\kappa}_i^{m+1} := -\partial_{ss}(\vec{x}_i^m + \Delta t_m \vec{v}_i^{m+1}).$$

To derive a weak formulation, we first write the above equations in terms of the weighted curvature

$$(3.13) \quad \tilde{\kappa}_i := \tilde{\gamma}\kappa_i$$

and then proceed similarly as in [10]: multiply (3.8), (3.9), (3.10), and (3.12) by test functions $\vec{\psi} \in \vec{H}^1(\Gamma_i)$ and $\psi \in H^1(\Gamma_i)$ and use integration by parts for the operator ∂_s . For simplicity we have hereafter dropped the superscript $m + 1$ for the unknowns. Furthermore, using the notation $\langle \cdot, \cdot \rangle$ for the L^2 inner product over the current interfaces Γ_i^m , we arrive at the following semi-implicit, time discrete set of equations.

PROBLEM 3.4. For $m = 1, 2, \dots$, find $\vec{\kappa}_i \in \vec{H}^1(\Gamma_i^m)$, $\tilde{\kappa}_i \in H^1(\Gamma_i^m)$, $v_i \in H^1(\Gamma_i^m)$, and $\vec{v}_i \in \vec{H}^1(\Gamma_i^m)$ such that

$$\begin{aligned} \langle \vec{\kappa}_i, \vec{\psi} \rangle - \Delta t_m \langle \partial_s \vec{v}_i, \partial_s \vec{\psi} \rangle &= \langle \partial_s \vec{x}_i^m, \partial_s \vec{\psi} \rangle & \forall \vec{\psi} \in \vec{H}^1(\Gamma_i^m), \\ \langle \tilde{\kappa}_i, \psi \rangle - \langle \tilde{\gamma} \tilde{\kappa}_i \cdot \vec{n}_i, \psi \rangle &= 0 & \forall \psi \in H^1(\Gamma_i^m), \\ \langle v_i, \psi \rangle + \langle \alpha \partial_s \tilde{\kappa}_i, \partial_s \psi \rangle + \beta \langle \tilde{\kappa}_i, \psi \rangle &= \langle \gamma_i, \psi \rangle & \forall \psi \in H^1(\Gamma_i^m), \\ \langle \vec{v}_i, \vec{\psi} \rangle - \langle v_i \vec{n}_i, \vec{\psi} \rangle &= 0 & \forall \vec{\psi} \in \vec{H}^1(\Gamma_i^m), \end{aligned}$$

where we have used the following abbreviations:

$$\alpha = \nu; \quad \beta = \frac{1}{\epsilon} \frac{\rho^*}{k_B T}; \quad \gamma_i = \frac{1}{\epsilon} (\rho - \rho^*).$$

Note that in the above formulation the adatom density ρ is needed only for computing γ_i . The discrete scheme can be written as a matrix-vector system by using a nodal basis as usual and is solved by a Schur complement approach; see [1] for details. Note that in contrast to [1] in the case of anisotropy, i.e., $\tilde{\gamma}$ and/or ν not being constant, we solve for the unknowns $\tilde{\kappa}_i$, $\tilde{\kappa}_i$, v_i , and \vec{v}_i rather than for κ_i , $\vec{\kappa}_i$, v_i , and \vec{v}_i .

The subproblem of boundary evolution consists of solving N decoupled problems for each interface $\Gamma_{i,h}$, $i = 1, \dots, N$. For the adatom diffusion problem the new interfaces $\Gamma_{i,h}^{m+1}$ and their weighted curvatures $\tilde{\kappa}_{i,h}$ will enter.

3.3. Implementation. The numerical method is implemented using ALBERT, an adaptive finite element software for scientific computation [25]. The program for the 2d adatom diffusion and that for the 1d boundary evolution are coupled via TCP/IP. The matrices are assembled using the standard assembling tools of ALBERT, except for the matrices involving line integrals. For the latter see [1].

Adaptivity for adatom diffusion. To obtain satisfactory computational results, a mesh with a sufficiently fine resolution near the moving island boundaries is needed. Thus it is indispensable to use some adaptive strategy for local mesh refinement and coarsening. As described in [1] we use an L^2 -like error indicator for local mesh coarsening and a purely geometric criterion for refinement, ensuring that the mesh size of the 2d grid at the moving boundaries is at least as fine as the 1d mesh size.

Adaptivity for boundary evolution. The 1d finite element meshes for the boundaries are also adapted. Nodes are inserted or removed from the current mesh in each time step according to the criterion that the distance between neighboring nodes is almost a constant.

Time adaptivity. In addition to adaptivity in space, adaptivity in time is also applied. The criteria for choosing the next time step results from the solution of the 1d problem. The boundaries are not allowed to sweep over a whole 2d element within one time step.

Algorithm. Combining the methods described so far we arrive at the following algorithm.

ALGORITHM 3.3. Let the initial boundaries $\Gamma_{i,h}^0$ be given. Set $m = 0$.

1. compute curvature $\kappa_{i,h}^0$ of the initial boundaries

2. compute initial adatom density ρ_h^0
 - (a) compute ρ_h^0
 - (b) compute $\gamma_i = \gamma_i(\rho_h^0)$
3. compute free boundaries $\Gamma_{i,h}^{m+1}$ and curvatures $\kappa_{i,h}^{m+1}$
 - (a) compute $v_{i,h}^{m+1}$, $\vec{v}_{i,h}^{m+1}$, and $\Gamma_{i,h}^{m+1}$
 - (b) refine and coarsen $\Gamma_{i,h}^{m+1}$
 - (c) compute $\kappa_{i,h}^{m+1}$ on $\Gamma_{i,h}^{m+1}$
4. compute adatom density ρ_h^{m+1}
 - (a) refine and coarsen \mathcal{T}_h^m
 - (b) compute ρ_h^{m+1}
 - (c) compute $\gamma_i = \gamma_i(\rho_h^{m+1})$
5. set $m := m + 1$, go to step 3.

4. Numerical results. We first present numerical results for the purely geometric motion of curves in section 4.1. In section 4.2 we then investigate numerically the isotropic growth of a single circular island and compare the numerical results with the known analytical solutions. The influence of anisotropic edge diffusion on the growth of a single island is shown in section 4.3. An example for several islands is shown in section 4.4. Further examples are concerned with decay and coarsening. Here the deposition flux F is turned off. In section 4.5 the decay of a crystalline cone is simulated and compared with the corresponding numerical solution of a system of ODEs for the radii of the islands, and in section 4.6 a large-scale simulation of Ostwald ripening of monolayer islands is presented.

Anisotropies will be described in terms of a function $f(\theta)$, $0 \leq \theta \leq 2\pi$, such that

$$(4.1) \quad \tilde{\gamma}(\theta) = \gamma_0(f(\theta) + f''(\theta)),$$

where we consider anisotropies of the type

$$f(\theta) = 1.0 + A \cos(k\theta),$$

with A being the strength of the anisotropy and k the periodicity. Thus, for $\tilde{\gamma}$ to be positive, it is necessary that $(k^2 - 1)A < 1$.

Unless otherwise stated, we use the following data in all numerical simulations:

- parameters: $D = 10^5$, $F = 1$, $\rho^* = 10^{-4}$, $\tau^{-1} = 0$, $\tilde{\gamma} = \gamma_0 = 0.3$, $\nu = 10$, $k_B T = 1$;
- domain: Ω is a circular domain with radius 10;
- mesh size of the initial 1d finite element mesh: $h \approx 0.05$;
- time step: $\Delta t = 10^{-4}$.

4.1. Geometric motion of curves. Our first test example is the purely geometric motion of curves governed by Problem 3.4 in section 3.2, decoupled from the adatom diffusion. Considering a single curve Γ , we may write (3.6) as

$$(4.2) \quad v = \gamma_i - \beta \frac{\tilde{\gamma} \kappa_i}{k_B T} + \partial_s(\nu \partial_s(\tilde{\gamma} \kappa_i)),$$

where γ_i is a function on the curve Γ , $\beta \geq 0$ is a constant, and $\tilde{\gamma}, \nu$ are positive functions of a single variable $0 \leq \theta \leq 2\pi$ denoting the angle of the outer normal of Γ with the x_1 -axis.

Choosing $\tilde{\gamma}$, ν , β , and γ_i in a suitable way, (4.2) and therefore the algorithm described in section 3.2 can be used to describe several geometric evolution equations.

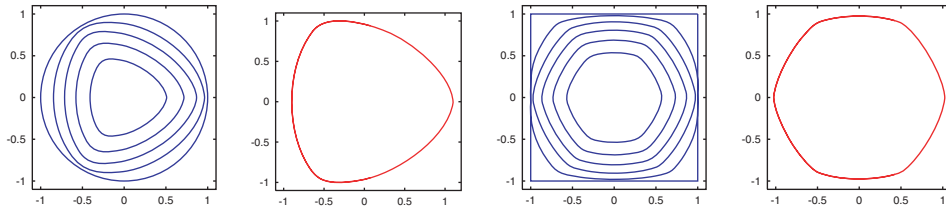


FIG. 1. *Anisotropic mean curvature flow: starting with a circle and anisotropy $f(\theta) = 1.0 + 0.1 \cos(3\theta)$; snapshots at $t = 0.0$, $t = 0.1$, $t = 0.2$, $t = 0.3$, and $t = 0.4$ and corresponding Wulff shape (left); starting with a square and anisotropy $f(\theta) = 1.0 + 0.025 \cos(6\theta)$; snapshots at $t = 0.0$, $t = 0.1$, $t = 0.2$, $t = 0.3$, $t = 0.4$, and $t = 0.5$ and corresponding Wulff shape (right).*

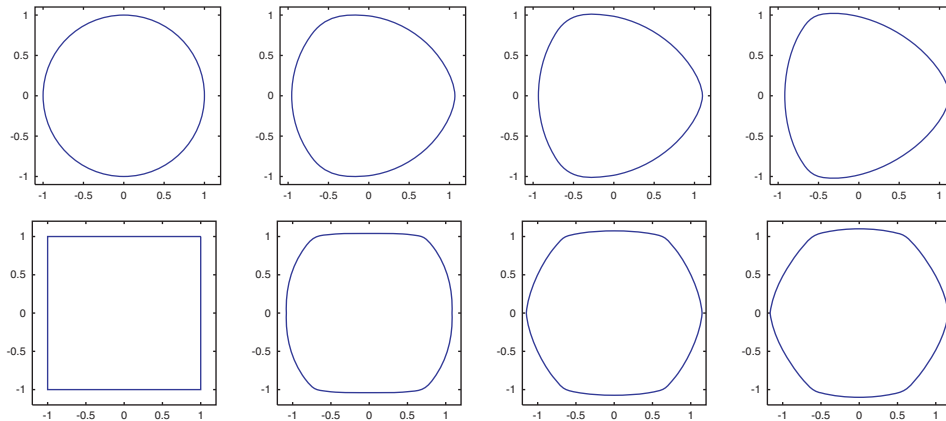


FIG. 2. *Anisotropic (1d) surface diffusion: starting with a circle and anisotropy $f(\theta) = 1.0 + 0.1 \cos(3\theta)$ (first row); starting with a square and anisotropy $f(\theta) = 1.0 + 0.025 \cos(6\theta)$ (second row); snapshots at $t = 0.0$, $t = 0.01$, $t = 0.02$, and $t = 0.1$.*

We will consider the following two examples:

- weighted mean curvature flow: $\nu = 0$, $\beta \neq 0$, $\tilde{\gamma} \neq 0$, and $\gamma_i = 0$;
- weighted edge diffusion: $\nu = 1$, $\beta = 0$, $\tilde{\gamma} \neq 0$, and $\gamma_i = 0$.

The smoothing properties of the mean curvature flow and of the surface diffusion have already been presented in [1] for the isotropic case. Here we will give some examples of anisotropic flows.

For the anisotropic surface free energy $A_\gamma(\Gamma) = \int_\Gamma \gamma$ the corresponding Wulff shape \mathcal{W}_γ is defined by

$$\mathcal{W}_\gamma = \{\vec{x} \in \mathbb{R}^2 \mid \vec{x} \cdot \vec{n} \leq \gamma(\vec{n}(\theta)) \forall \vec{n} \in \mathbb{R}^2, |\vec{n}| = 1\}.$$

The weighted curvature $\tilde{\kappa} = \tilde{\gamma}\kappa$ is constant on \mathcal{W}_γ and the Wulff shape minimizes the 1d surface free energy under the constraint of fixed area. Therefore, \mathcal{W}_γ describes the equilibrium shape in the case of anisotropy. For this reason one expects the edge-diffusion flow to tend to the Wulff shape as a stationary solution and the mean curvature flow to shrink a given curve towards the (rescaled) Wulff shape. Our numerical experiments agree perfectly with this consideration, as can be seen in Figure 1 and Figure 2. We have chosen two different anisotropies f with periodicity 3 and 6, respectively. The corresponding Wulff shapes are depicted in Figure 1. The convergence towards the Wulff shape is investigated quantitatively by calculating an

TABLE 1

Approximate Hausdorff distance between the numerical solution and the Wulff shape for various anisotropies. Initial curve is a square of area 4. The remaining error for time > 0.1 results from the constant mesh size of $h = 0.125$ and the natural approximation error of a continuous curve by linear segments.

Time	$k = 3,$	$k = 3,$	$k = 4,$	$k = 4,$	$k = 5,$	$k = 5,$
	$A = 1/16$	$A = 1/8$	$A = 1/30$	$A = 1/15$	$A = 1/48$	$A = 1/24$
0.0	0.2420	0.2880	0.2290	0.2520	0.2150	0.2300
0.01	0.1110	0.1610	0.0749	0.1100	0.0599	0.0930
0.02	0.0450	0.0990	0.0223	0.0382	0.0179	0.0267
0.1	0.0121	0.0438	0.0077	0.0222	0.0074	0.0175
0.5	0.0121	0.0434	0.0077	0.0222	0.0074	0.0177

approximate Hausdorff distance between the numerical curve and the Wulff shape. The Hausdorff distance is approximated by first measuring the distance of a grid point on the curve to the intersection point of the straight line connecting the grid point and the origin with the Wulff shape and then taking the maximum over all grid points on the curve. The results for anisotropic surface diffusion for the evolution of a square to a three-, four-, and five-fold symmetry ($k = 3, 4, 5$) with a strength of the anisotropy A chosen to satisfy $(k^2 - 1)A \leq 1$ are given in Table 1. If $(k^2 - 1)A = 1$, the equation becomes singular, and corners occur in the Wulff shape. Also this situation can be handled within the described algorithm. The convergence of the curve towards its stationary Wulff shape is clearly shown.

4.2. Growth of a single circular island. We consider a single circular island $\Omega_1(t)$ of radius $R(t)$ at time t that is growing on a terrace, which is a concentric circular region with radius R_Ω . In the quasi-stationary approximation for the adatom diffusion, the time dependence in the diffusion equation (2.1) is dropped. This approximation is valid if $F/D \ll 1$. Since $F/D = 10^{-5} \ll 1$, we expect our simulation of the time-dependent diffusion equation to be in good agreement with the analytic solution of the quasi-stationary diffusion equation.

Using polar coordinates (r, θ) with the origin at the center of the circular island, the radially symmetric solution of the quasi-stationary diffusion equation is given by [16]

$$\begin{aligned}\rho_1(r, t) &= \frac{F}{4D} (R(t)^2 - r^2) + \rho^* \left(1 + \frac{\tilde{\gamma}}{k_B T R(t)} \right), \\ \rho_0(r, t) &= \frac{F}{4D} (R(t)^2 - r^2) + \frac{F R_\Omega^2}{2D} \ln \left(\frac{r}{R(t)} \right) + \rho^* \left(1 + \frac{\tilde{\gamma}}{k_B T R(t)} \right).\end{aligned}$$

Since the curvature $\kappa_1 = 1/R(t)$ of the circular boundary $\Gamma_1(t)$ is spatially constant, we have $\partial_{ss}\kappa_1 = 0$. Furthermore, since the velocity of the circular boundary $\Gamma_1(t)$ is given by $v_1 = R'(t)$, by a simple calculation we get $R'(t) = F R_\Omega^2 / (2R(t))$, i.e., $(R(t)^2)' = F R_\Omega^2$. Thus, we obtain the dynamic law

$$(4.3) \quad R(t)^2 = F R_\Omega^2 t + R(0)^2$$

for the evolution of the circular boundary $\Gamma_1(t)$.

For the simulation we have chosen an island with initial radius $R(0) = 3.0$ growing on a terrace of radius $R_\Omega = 10.0$. From Figure 3, showing the adaptively refined 2d mesh, the computed 1d boundary $\Gamma_{1,h}$, and the computed adatom density ρ_h at various times, it can be seen that the evolution of the growing island is very stable.

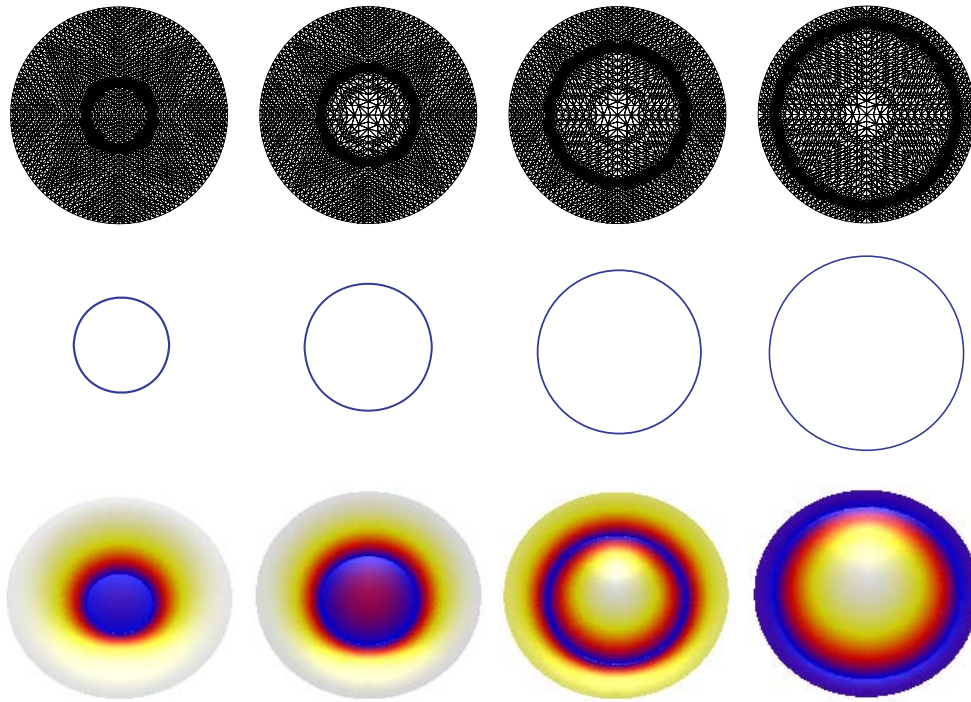


FIG. 3. 2d mesh, 1d boundary, and adatom density at time instants $t = 0.0, 0.1, 0.3,$ and 0.6 .

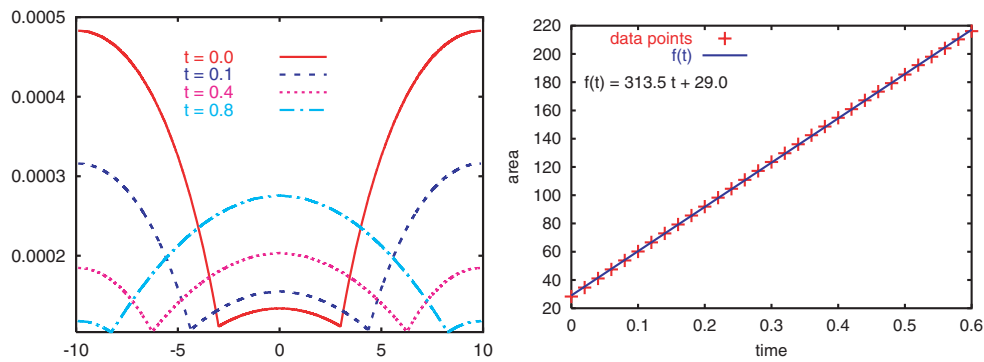


FIG. 4. Adatom density profile of the numerical solution (left) and area growth rate (right). The function f is a least square fit of the data to an affine linear function.

As a test of mass balance, the growth rate of the island area is depicted in Figure 4 (right). Evaluating (4.3), one expects a growth rate of $F|\Omega| \approx 314.15$. The simulations are in good agreement with this value, as shown by a least square fit of the numerical data; see Figure 4 (right). Figure 4 (left) shows the profile of the adatom density at the same time instants as in Figure 3.

Finally, in Figure 5, the numerical and analytical solutions are compared by depicting the relative error of the adatom density along the x_1 -axis for the same time instants as in Figure 4. The maximum relative pointwise error is less than 2% over the whole time period. We conclude that the numerical algorithm is fairly accurate

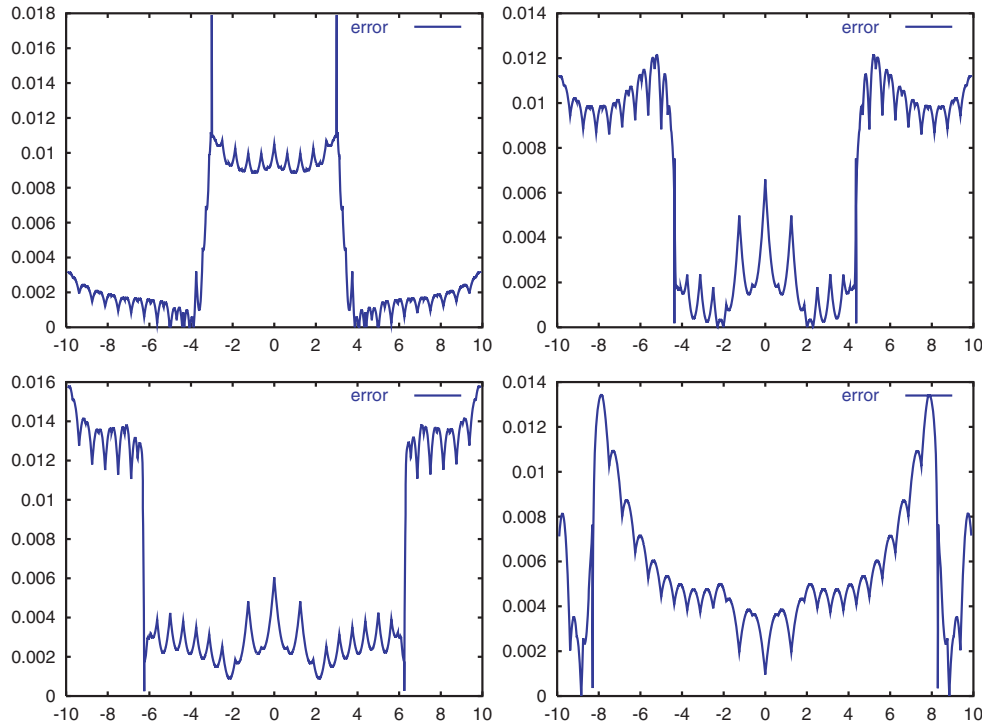


FIG. 5. Relative pointwise error of the numerical solution at time instants $t = 0.0, 0.1, 0.3,$ and 0.6 .

for describing both the free boundary evolution and the adatom diffusion equation.

4.3. Anisotropic growth of a single island. In this example we investigate the influence of the edge diffusion on anisotropic growth. We simulate the anisotropic growth of a single island with anisotropy given by

$$f(\theta) = 1.0 + 0.1 \cos 3\theta,$$

both without edge diffusion (i.e., $\nu = 0$) and with edge diffusion ($\nu = 10.0$) and compare the respective results. Starting with a circle, we expect the island to at least resemble the corresponding Wulff shape (see Figure 1) in both cases. The simulated evolutions of the moving boundaries are shown in Figure 6. Comparing the two figures, it is seen that edge diffusion drives the evolution of the boundary towards the Wulff shape.

4.4. Evolution of a wedding cake. The next example is a growing “wedding cake.” We consider three circular islands with radii $R(1) = 7.0$, $R(2) = 5.0$, and $R(3) = 3.0$ sitting on top of each other and growing on a circular substrate of radius $R_\Omega = 10.0$.

As in the case of one circular island (see Figure 4 (right)), we have calculated the area growth rate using a least square fit yielding a growth rate of 316.8, which again is in good agreement with the expected value $F|\Omega| \approx 314.4$. In Figure 7 we show the discrete height function at various times. The discrete height function was obtained by marking the elements of the 2d mesh by the height, i.e., the index i (number of

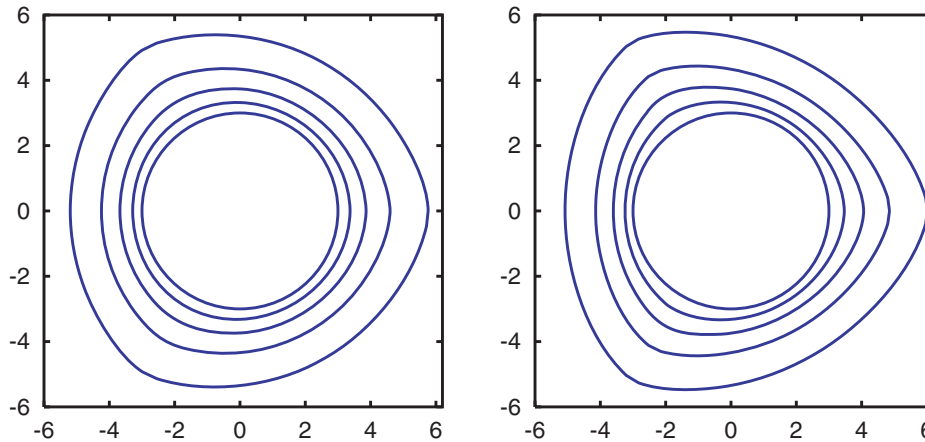


FIG. 6. Anisotropic growth of a single island with anisotropy $f(\theta) = 1.0 + 0.1 \cos 3\theta$. Moving boundary at time instants $t = 0.0, 0.02, 0.05, 0.1,$ and 0.2 (from inner to outer curve). Left: without (1d) surface diffusion; right: with (1d) surface diffusion.

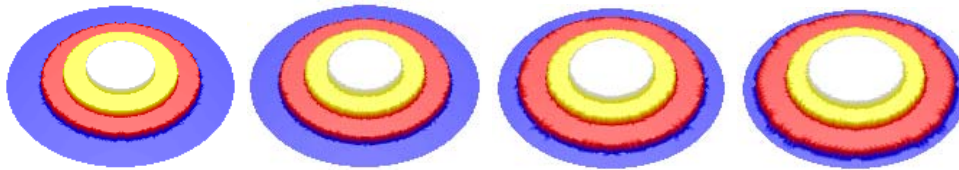


FIG. 7. Discrete height function of the wedding cake at time instants $t = 0.0, 0.1, 0.3,$ and 0.5 .

atomic layers) of the corresponding terrace. If the boundary Γ_i intersects the element, it is marked by $i + \frac{1}{2}$.

The adatom density profile is represented in Figure 8.

4.5. Decay of a crystalline cone. As a numerical benchmark, which also includes the simple-to-handle topological changes of disappearances of terraces, we consider the decay of a crystalline cone in a rotational symmetric and in a particular isotropic setting, which allows us to compare the simulations with an ODE calculation. As in section 4.4 the initial configuration is a wedding cake, now consisting of 10 concentric circular islands sitting on top of each other; see Figure 9 (left). Denoting the radius of the i th layer by $R_i(t)$, the initial configuration is given by $R_i(0) = 11 - i$. To study the decay of this cone, the deposition flux F in (2.1) is set to zero. We note that the decay of the whole wedding cake takes a very long time. Also the velocities of the island boundaries vary over some orders of magnitude, since the velocity of the boundary of a very small island (just before it disappears) becomes very large. Thus, it is indispensable to use adaptivity in time.

Since the diffusion coefficient D is very large, we may benchmark our numerical results by comparing the simulations with an ODE simulation of the corresponding quasi-stationary approximation. In polar coordinates, the diffusion equation becomes

$$(4.4) \quad \rho''(r) + \frac{1}{r} \rho'(r) = 0, \quad r \neq R_i,$$

$$(4.5) \quad \rho(R_i) = \rho^* \left(1 + \frac{\mu}{R_i} \right), \quad \mu = \frac{\gamma}{k_B T}.$$

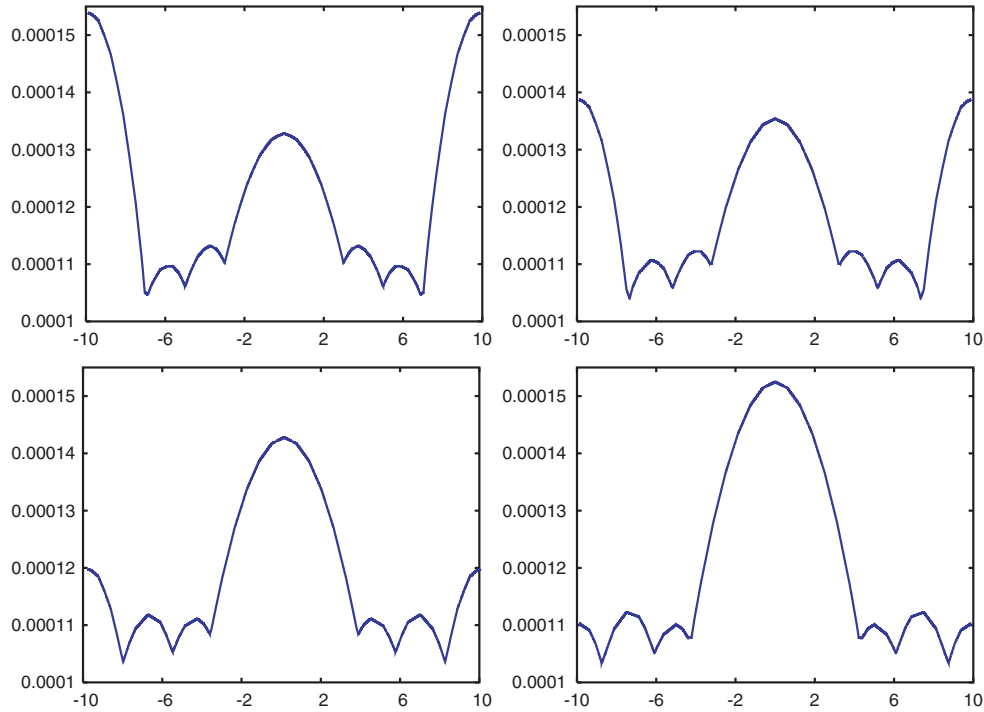


FIG. 8. Adatom density profile of the wedding cake on a cut along the x_1 -axis at times $t = 0.0, 0.1, 0.3,$ and 0.5 .

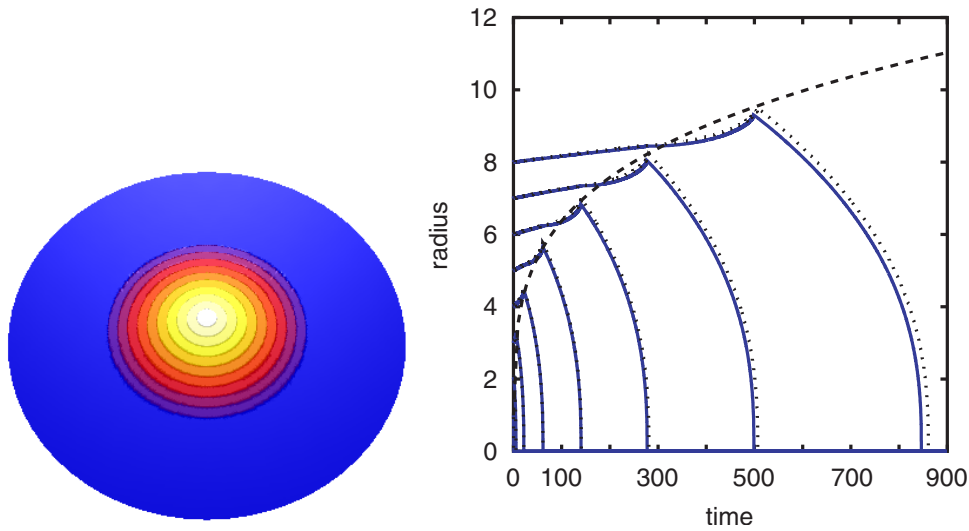


FIG. 9. Discrete height function of initial configuration of a circular crystalline cone (left). Time evolution of step radii (right): finite element simulation (solid), rotational symmetric solution (dotted), and fitted facet edge radius ($r = (16.46t + 1.0)^{1/4}$) (dashed).

This system can be solved explicitly (given the radii $R_i(t)$) and that one obtains a coupled system of ODEs for the velocities $v_i = \dot{R}_i(t)$ from (2.3) (see [13]). This

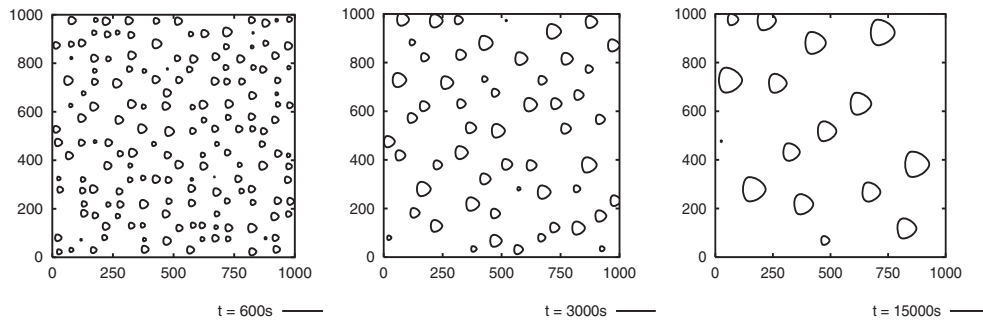


FIG. 10. Anisotropic ripening with anisotropy $\gamma(\theta) = 1.0 + 0.1 \cos(3\theta)$ and coverage $\phi = 0.085$. Initial configuration: 400 islands on a substrate of size 1000×1000 . Island boundaries at times $t = 600s$, $3000s$, and $15000s$.

coupled system of ODEs is numerically integrated and compared with the full finite element solution. The time evolutions of the step radii both for the full finite element solution and the rotational symmetric solution are shown in Figure 9 (right).

As expected, the uppermost island shrinks while the outer steps expand and absorb the adatoms emitted by the shrinking island. When the uppermost island disappears, the next island starts shrinking, and so on. This process results in a propagating *effective* front, given by the radius of the uppermost island at the moment, when the previously uppermost island disappears; see Figure 9. The position of the front behaves like $R_{front} \sim t^{1/4}$, as shown by the dashed line in Figure 9, which is in agreement with the analytical results for the decay of an infinite crystalline cone obtained in [13].

4.6. Ostwald ripening of monolayer islands. As a final example, we present a large-scale simulation of Ostwald ripening of monolayer islands on a substrate. Considering an ensemble of monolayer islands of different sizes on a substrate, the drift of the system to minimize the curvature-dependent step-free energy associated with the island boundaries provides a thermodynamic driving force for large islands to grow at the expense of small ones, which finally disappear. Thus the number of islands is decreasing, while the average island size increases. Such a coarsening behavior is called Ostwald ripening. We consider 400 islands on a substrate of size 1000×1000 in the low coverage regime (i.e., the total area of the islands is small compared to that of the substrate) and study the ripening process. As in the last example, the deposition flux F is zero. Periodic boundary conditions are used. Some snapshots of ripening with anisotropic edge energy are depicted in Figure 10, showing the island edges at various times. To investigate the scaling law for the average island size, a log-log plot of the average island radius (isotropic edge energy) versus time is shown in Figure 11. To get a statistically meaningful result, we averaged over 5 runs with different initial distributions of 400 islands with coverage 0.085. An affine linear fit in the asymptotic regime ($\ln(t) > 6.0$) yields a slope of 0.33, which is in excellent agreement with the asymptotic scaling law $r \sim t^{1/3}$ derived by LSW theory [17, 27].

5. Conclusions. In this work, we have developed an adaptive finite element method for the simulation of island dynamics in epitaxial growth of thin films in the diffusion limited regime. Our model is a free (or moving) boundary-type problem that consists of the diffusion equation for the adatom density and the boundary evolution equation that determines the normal velocity of the steps. Special emphasis was placed

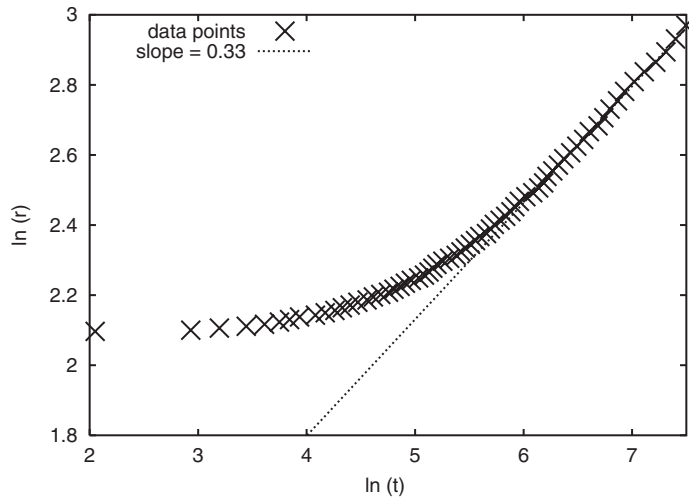


FIG. 11. *Scaling of average island radius r : Log-log plot of the average island radius over time and affine linear fit in the asymptotic regime ($\ln(t) > 6.0$).*

on the treatment of anisotropic edge diffusion. While our method cannot handle non-trivial topological changes at the present stage, it has the advantage of exploiting the variational structure of the model and resolving the fourth-order geometric evolution law for the moving boundaries in an efficient manner. The method is tested by comparing with analytical and ODE solutions. Moreover, further more realistic examples of long-time and large-scale simulations confirm the efficiency of the method.

REFERENCES

- [1] E. BÄNSCH, F. HAUSSER, O. LAKKIS, B. LI, AND A. VOIGT, *Finite element method for epitaxial growth with attachment-detachment kinetics*, J. Comput. Phys., 194 (2004), pp. 409–434.
- [2] E. BÄNSCH, P. MORIN, AND R. H. NOCHETTO, *A finite element method for surface diffusion: The parametric case*, J. Comput. Phys., 203 (2005), pp. 321–343.
- [3] W. K. BURTON, N. CABRERA, AND F. C. FRANK, *The growth of crystals and the equilibrium of their surfaces*, Philos. Trans. Roy. Soc. London Ser. A, 243 (1951), pp. 299–358.
- [4] R. E. CAFLISCH, W. E. M. F. GYURE, B. MERRIMAN, AND C. RATSCH, *Kinetic model for a step edge in epitaxial growth*, Phys. Rev. E (3), 59 (1999), pp. 6879–6887.
- [5] R. E. CAFLISCH, M. F. GYURE, B. MERRIMAN, S. OSHER, C. RATSCH, D. VVEDENSKY, AND J. ZINK, *Island dynamics and the level set method for epitaxial growth*, Appl. Math Lett., 12 (1999), pp. 13–22.
- [6] R. E. CAFLISCH AND B. LI, *Analysis of island dynamics in epitaxial growth of thin films*, Multiscale Model. Simul., 1 (2003), pp. 150–171.
- [7] S. CHEN, B. MERRIMAN, M. KANG, R. E. CAFLISCH, C. RATSCH, L.-T. CHENG, M. GYURE, R. P. FEDKIW, C. ANDERSON, AND S. OSHER, *Level set method for thin film epitaxial growth*, J. Comput. Phys., 167 (2001), pp. 475–500.
- [8] P. CIARLET, *The Finite Element Method for Elliptic Problems*, North-Holland, Amsterdam, 1978.
- [9] U. CLARENZ, F. HAUSSER, A. VOIGT, AND U. WEIKARD, *Level set method for fourth order problems*, in Multiscale Modeling in Epitaxial Growth, A. Voigt, ed., Birkhäuser, Basel, 2005, pp. 227–238.
- [10] G. DZIUK, *An algorithm for evolutionary surfaces*, Numer. Math., 58 (1991), pp. 603–611.
- [11] R. GHEZ AND S. S. IYER, *The kinetics of fast steps on crystal surfaces and its application to the molecular beam epitaxy of silicon*, IBM J. Res. Develop., 32 (1988), pp. 804–818.
- [12] M. F. GYURE, C. RATSCH, B. MERRIMAN, R. E. CAFLISCH, S. OSHER, J. ZINCK, AND D. VVEDENSKY, *Level-set method for the simulation of epitaxial phenomena*, Phys. Rev. E (3), 58 (1998), pp. R6927–R6930.

- [13] N. ISRAELI AND D. KANDEL, *Profile of a decaying crystalline cone*, Phys. Rev. B (3), 60 (1999), pp. 5946–5962.
- [14] A. KARMA AND M. PLAPP, *Spiral surface growth without desorption*, Phys. Rev. Lett., 81 (1998), pp. 4444–4447.
- [15] J. KRUG, *Four lectures on the physics of crystal growth*, Phys. A, 318 (2002), pp. 47–82.
- [16] B. LI, A. RÄTZ, AND A. VOIGT, *Stability of a circular epitaxial island*, Phys. D, 198 (2004), pp. 231–247.
- [17] I. M. LIFSHITZ AND V. V. SLYOZOV, *The kinetics of precipitation from supersaturated solid solutions*, J. Phys. Chem. Solids, 19 (1961), pp. 35–50.
- [18] F. LIU AND H. METIU, *Stability and kinetics of step motion on crystal surfaces*, Phys. Rev. E (3), 49 (1994), pp. 2601–2616.
- [19] M. PETERSON, C. RATSCH, R. E. CAFLISCH, AND A. ZANGWILL, *Level set approach to reversible epitaxial growth*, Phys. Rev. E (3), 64 (2001), 061602.
- [20] A. PIMPINELLI AND J. VILLAIN, *Physics of Crystal Growth*, Cambridge University Press, Cambridge, UK, 1998.
- [21] C. RATSCH, M. F. GYURE, R. E. CAFLISCH, F. GIBOU, M. PETERSON, M. KANG, J. GARCIA, AND D. D. VVEDENSKY, *Level-set method for island dynamics in epitaxial growth*, Phys. Rev. B (3), 65 (2002), 195403.
- [22] A. RÄTZ AND A. VOIGT, *Phase-field model for island dynamics*, Appl. Anal., 83 (2004), pp. 1015–1026.
- [23] A. RÄTZ AND A. VOIGT, *Phase-field model for island dynamics with edge-diffusion*, in Multi-scale Modeling in Epitaxial Growth, A. Voigt, ed., Birkhäuser, Basel, 2005, pp. 69–96.
- [24] A. SCHMIDT, *Computation of three dimensional dendrites with finite elements*, J. Comput. Phys., 125 (1996), pp. 293–312.
- [25] A. SCHMIDT AND K. G. SIEBERT, *ALBERT — software for scientific computations and applications*, Acta Math. Univ. Comenian. (N.S.), 70 (2000), pp. 105–122.
- [26] P. SMEREKA, *Semi-implicit level set methods for curvature and surface diffusion motion*, J. Sci. Comput., 19 (2003), pp. 439–456.
- [27] C. WAGNER, *Theorie der Alterung von Niederschlägen durch Umlösen (Ostwald-Reifung)*, Z. Elektrochemie, 65 (1961), pp. 581–591.